THE ASTROPHYSICAL JOURNAL, 569:322–333, 2002 April 10

THE ROLE OF OUTFLOWS AND C SHOCKS IN THE STRONG DEUTERATION OF L1689N

D. C. LIS,[1] M. GERIN,[2] T. G. PHILLIPS,[1] AND F. MOTTE[1]

Received 2001 October 11; accepted 2001 December 14

ABSTRACT

Recent detections of doubly deuterated ammonia and formaldehyde in L134N and L1689N have renewed interest in deuterium fractionation in cold, dense molecular gas. Chemical models show that the level of fractionation depends critically on the physical conditions, namely, the temperature and density of the molecular gas. Therefore, detailed studies of cold, dense molecular cores are required to constrain the existing chemical networks. We have mapped the core of the remarkable star-forming molecular cloud L1689N in a number of molecular tracers, including singly deuterated species, in order to obtain detailed information on the morphology and kinematics of the molecular gas, as well as the physical conditions in the dense core and the shocked regions associated with the molecular outflows emanating from the embedded far-infrared source IRAS 16293–2422. Our data suggest the presence of two regions of interaction between the molecular outflows and the dense ambient cloud, one of them associated with the SiO peak E1, the other one near the peak of deuterated and doubly deuterated molecular species ~90″ east of the *IRAS* source. The observed intensities of the CO (3–2), (4–3), and (6–5) emission at these two locations are consistent with those predicted by C shock models with velocities of 15–25 and 8–10 km s^{-1}, respectively. The relatively low shock velocity derived for the deuterium peak explains why no SiO emission has been detected at this location. Deuterated molecular species, such as DCO^+ and DCN, in the core of L1689N are kinematically and morphologically distinct from other molecular tracers of the dense gas, such as HCO^+, $H^{13}CO^+$, and HCN. The peak of deuterated molecules is also displaced from the extended millimeter dust continuum source located in this region. We use formaldehyde observations to derive the excitation conditions in the dense gas and, subsequently, the D/H ratios in HCO^+ and HCN at several locations via large velocity gradient modeling. These ratios are typically ~1% toward the locations of the *IRAS* source and the SiO peak E1, with much higher values, ~10%, derived toward the deuterium peak. These values fall within the range of predictions of gas-phase chemical models for dense and cold gas, provided that significant accretion of H_2O, CO, and other molecular species on the dust grains has occurred. However, some discrepancies between the observations and model predictions remain. For example, contrary to gas-phase model predictions, we derive a higher deuterium fractionation in HCN compared to HCO^+.

Subject headings: astrochemistry — ISM: abundances — ISM: individual (L1689N) — ISM: jets and outflows — ISM: molecules — stars: formation

On-line material: color figures

1. INTRODUCTION

Among the dark clouds in the Ophiuchus region, the dense core L1689N (e.g., Wootten & Loren 1987; Loren, Wootten, & Wilking 1990) is remarkable in that it harbors a young protostar, two molecular outflows, and a cold, nearby molecular core. The bipolar outflows both originate from the far-infrared source IRAS 16293–2422 (Mizuno et al. 1990 and references therein). This object has also been the subject of much discussion as a probable example of gas infall (e.g., Walker et al. 1986). High-resolution interferometric observations have revealed that this protostar is in fact a young binary system (Wootten 1989; Mundy et al. 1992). The protostellar sources are still deeply embedded in a dense molecular envelope, giving rise to an active chemistry (Ceccarelli et al. 2000a). Surveys of millimeter emission lines have revealed the presence of complex molecules in the hot core surrounding the binary system (Blake et al. 1994; van Dishoeck et al. 1995; Ceccarelli et al. 2000b). However, heating from the embedded protostars affects only a small fraction of the dense core, with most of the molecular mass remaining relatively cold. Optically thick lines of CO, SiO, HCN, and HCO^+ show a pronounced self-reversal at the systemic velocity, ~3.8 km s^{-1}. Menten et al. (1987) derive a mean density of (2–3) × 10^4 cm^{-3} in the parent molecular cloud and a kinetic temperature of 12 K, based on their ammonia observations.

The generic name of the molecular core surrounding IRAS 16293–2422 is L1689N. Recently, this dark cloud has also been referred to as Oph E, owing to its location to the east of the main Ophiuchus cloud. However, this name should be avoided, as it may be confused with the dense core in the main Ophiuchus cloud, labeled ρ Oph E (see, e.g., Loren et al. 1990). Thus, we use consistently throughout this paper the name L1689N for the dense molecular cloud surrounding IRAS 16293–2422.

Large-scale maps of millimeter lines and the continuum emission have revealed a second dense core, ~90″ east of the IRAS source, with high abundances of ammonia and deuterated species (Wootten & Loren 1987; Gerin et al. 1987; Shah & Wootten 2001; Saito et al. 2000; Hirota, Ikeda, & Yamamoto 2001). The recent detection of doubly deuterated molecules in L1689N, D_2CO toward both the *IRAS* source and the nearby cold dense core, and ND_2H toward the latter source (Loinard et al. 2000, 2001; Ceccarelli et al.

[1] California Institute of Technology, Downs Laboratory of Physics 320-47, Pasadena, CA 91125; dcl@submm.caltech.edu.

[2] Radioastronomie Millimétrique-UMR 8540 du CNRS, Laboratoire de Physique de l'ENS, 24 Rue Lhomond, 75231 Paris Cedex 05, France.

2001) has renewed interest in this cloud. High levels of deuterium fractionation are found for both singly deuterated species ($[NH_2D]/[NH_3] = 7\%$–9%, Loinard et al. 2001; Shah & Wootten 2001; A. Wootten, J. G. Mangum, & L. G. Mundy 2002, in preparation; $[DNC]/[HNC] = 9\%$, Hirota et al. 2001) and doubly deuterated species ($[D_2CO]/[H_2CO] = 40\% \pm 20\%$ toward the cold core; Loinard et al. 2001). The origin of the high level of deuterium fractionation is uncertain. Whereas high deuterium fractionation for molecular ions (HCO^+, N_2H^+) and some neutral species (NH_3) can be produced in cold, dense gas by the standard gas-phase ion-molecule chemistry (Roberts & Millar 2000a, 2000b; Rodgers & Charnley 2001), the extremely high fractionation of formaldehyde is best explained if the fractionation occurs on grain mantles (Ceccarelli et al. 2001). However, Roberts & Millar (2000b) have shown that, when accretion onto dust grains (depletion) is taken into account, doubly deuterated molecules may also be produced through gas-phase chemistry. In the presence of shocks associated with the molecular outflows, some species frozen on grains may be released into the gas phase. Indeed, extended SiO emission, which is often used as a shock tracer (e.g., Schilke et al. 1997), has been found in L1689N, although not at the deuterium peak (Hirano et al. 2001).

To better understand this complex molecular core and compare the observed deuterium fractionation with chemical models, accurate information on the physical conditions in the dense core and in the shocked regions associated with the molecular outflows is needed. In this paper we present additional millimeter and submillimeter spectroscopic data on L1689N, which help to refine the description of the physical conditions in different regions. CO (3–2), (4–3), and (6–5) data are used to constrain the gas density and temperature in the outflowing gas. The different morphological regions in L1689N are clearly separated in maps of the HCN, HCO^+, $H^{13}CO^+$, DCO^+, $C^{18}O$, and 1.3 mm dust continuum emission.

2. OBSERVATIONS

Spectroscopic observations of L1689N presented here were carried out between 2000 July and 2001 August using the facility receivers and spectrometers of the Caltech Submillimeter Observatory (CSO) on Mauna Kea, Hawaii. The data were taken under good to average weather conditions (225 GHz zenith opacity ~0.04–0.15). CSO main-beam efficiencies, determined from observations of planets, are 65%, 65%, 53%, and 40% for the 230, 345, 460, and 650 GHz receivers, respectively. Given the extended distribution of the CO emission (§ 3.1), we use a 60% efficiency for the 460 and 650 GHz CO lines, intermediate between the main-beam and Moon efficiencies. Typical calibration uncertainties are ~25%. The pointing of the telescope was determined from total power observations of Mars, located ~10° from L1689N, and was stable to within $\lesssim 5''$. We used both the 500 and 50 MHz bandwidth acousto-optical facility spectrometers. The two spectrometers gave internally consistent line intensities, typically within $\lesssim$5%–10%.

We obtained a $6' \times 6'$ on-the-fly (OTF) map of the CO (3–2) transition in L1689N with $10''$ pixel spacing using the 50 MHz spectrometer. The reference (0, 0) position for all maps presented here is $\alpha_{1950.0} = 16^h29^m27^s.6$, $\delta_{1950.0} = -24°22'33''$. Additional CO (3–2), (4–3), and (6–5) spectra were taken near the peak of deuterated molecules (see § 3.3), within the SiO source E1 (Hirano et al. 2001), and at the position of the *IRAS* source. We also obtained OTF maps of HCO^+ (3–2), $H^{13}CO^+$ (3–2), HCN (3–2), and DCO^+ (3–2) lines that cover the *IRAS* source, E1 shocked region, and the deuterium peak. In addition, spectra of the following molecular transitions were obtained at selected positions: H_2CO (3_{03}–2_{02}), (3_{23}–2_{21}), and (5_{05}–4_{04}); $H^{13}CN$ (3–2); DCN (3–2); DCO^+ (5–4); N_2D^+ (3–2) and (4–3); and $C^{18}O$ (2–1). The FWHM beam size of the CSO telescope varies between ~35″ at 218 GHz and ~11″ at 690 GHz.

3. DISCUSSION

3.1. CO *Emission and the Excitation Conditions in the Molecular Outflow*

Figure 1 shows channel maps of the CO (3–2) emission in L1689N. The observed morphology is consistent with previous lower angular resolution CO observations of this region (see Mizuno et al. 1990 and references therein), showing two outflows, both emanating from IRAS 16293−2422. Extended CO emission is present at the systemic velocity of the cloud (4 km s^{-1} panel), and two compact high-velocity redshifted peaks are seen at velocities $\gtrsim$8 km s^{-1}. These have been referred to as western red and northeastern red lobes in the previous studies. The blueshifted emission is generally weaker and more spatially extended than the redshifted emission, indicating an interaction between the outflows and the ambient cloud. Hirano et al. (2001) have studied the distribution of the SiO (2–1) emission in the vicinity of IRAS 16293−2422 and found significantly enhanced SiO emission in the northeastern red outflow lobe, as well as ~50″ east of the *IRAS* source (Fig. 1, *circle*; the position referred to as E1). They interpret the enhanced SiO emission at this location as evidence of a dynamical interaction between the northeastern red outflow lobe and the dense ambient cloud. They also conclude that the observed quadrupolar morphology of the high-velocity gas is a result of two separate bipolar outflows emanating from the *IRAS* source (Fig. 1, *triangle*). The position at which enhanced emission from deuterated species is observed is located within the eastern blue lobe of the outflow (Fig. 1, *square*), and strong blueshifted CO (3–2) emission with velocities down to −6 km s^{-1} is detected there.

Figure 2 shows CO (3–2), (4–3), and (6–5) spectra at the *IRAS*, E1, and deuterium peak positions. All the lines are clearly detected and show a self-reversal at the systemic velocity of the cloud. The integrated line intensities and velocity-averaged line ratios are given in Table 1. The two line ratios can be used to constrain the excitation conditions in the high-velocity molecular gas via large velocity gradient (LVG) modeling. We have computed a grid of LVG models with varying kinetic temperatures and H_2 volume densities and, for each value of the kinetic temperature and density, computed χ^2 values corresponding to the two observed line ratios. The results for the E1 position and the deuterium peak are shown in Figure 3 (*top and bottom panels*, respectively). In both cases, the observed line ratios are consistent with a wide range of densities and kinetic temperatures. Nevertheless, the χ^2 plot can be used to derive lower limits for the temperature and density *in the outflowing gas* (see Table 1). For gas densities $\gtrsim 1 \times 10^5$ cm^{-3}, best-fit kinetic

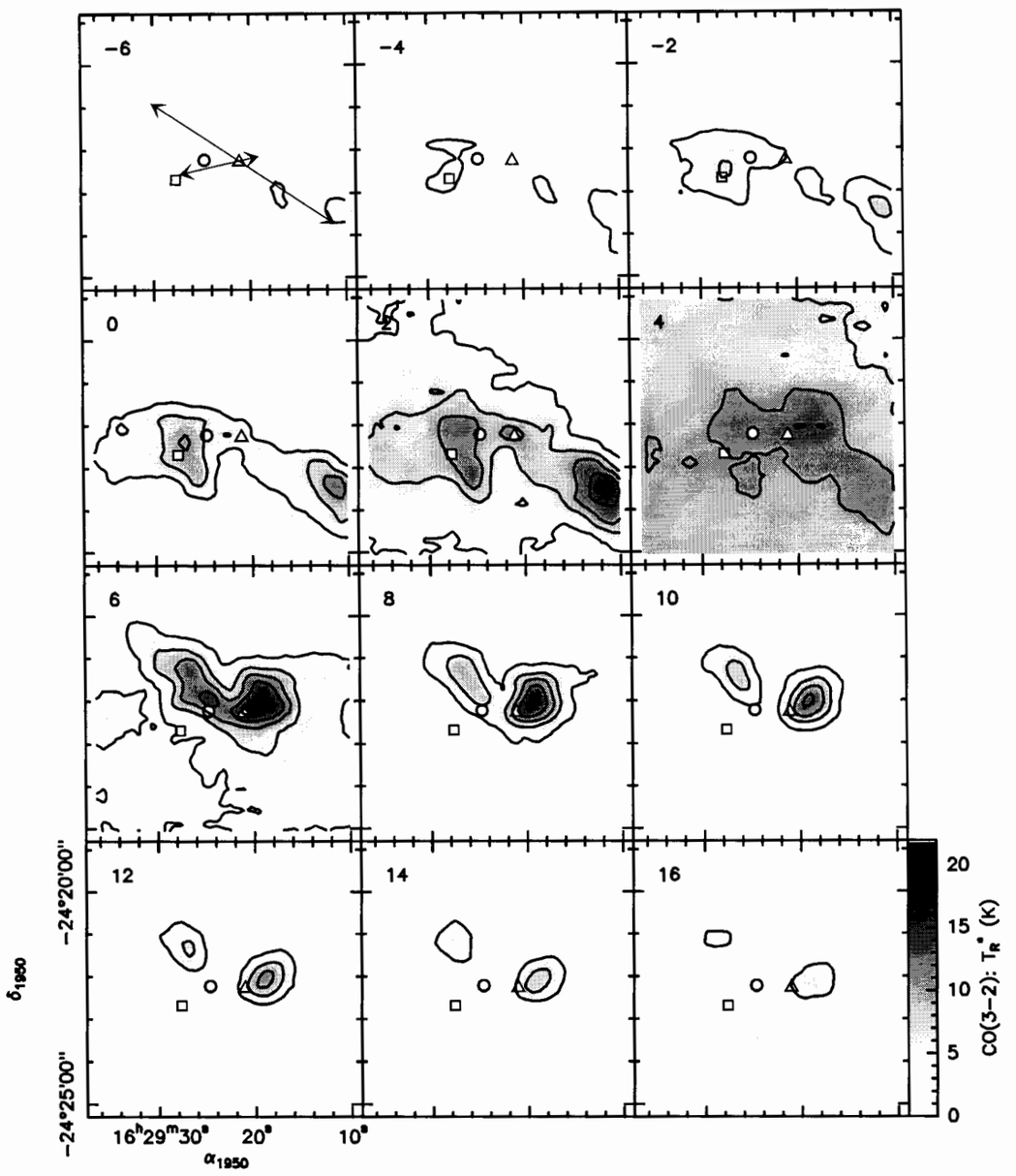

FIG. 1.—Channel maps of the CO (3–2) emission showing the quadrupolar outflow emanating from IRAS 16293–2422. Symbols mark the location of the *IRAS* source (*triangle*), the SiO peak E1 (*circle*; Hirano et al. 2001), and the DCO^+ peak (*square*; see Fig. 6, 3.5 km s^{-1} panel). Contour levels are from 2 to 18 K, with an interval of 4 K. Velocities are labeled in the upper left corner of each panel.

temperature values are ~30, 55, and 75 K for the deuterium peak, E1, and the *IRAS* position, respectively.

The asymmetric CO line profiles at the location of the deuterium peak are reminiscent of those predicted for shocked gas (C-type shocks). Given the location of the deuterium core within the eastern blue lobe of the outflow and the observed velocity shift of the deuterated species with respect to the systemic velocity (§ 3.3), it is plausible that both the E1 peak and the deuterium source are interaction regions between the outflow and the dense ambient gas. In this case, the observed intensities of the CO lines can be compared with predictions of C shock models and can be used to estimate the shock velocity. Draine & Roberge (1984) computed CO line intensities in shocked interstellar molecular clouds for a wide range of C-type shock velocities, v_s, and preshock gas densities, n_H^o. Their Figure 6

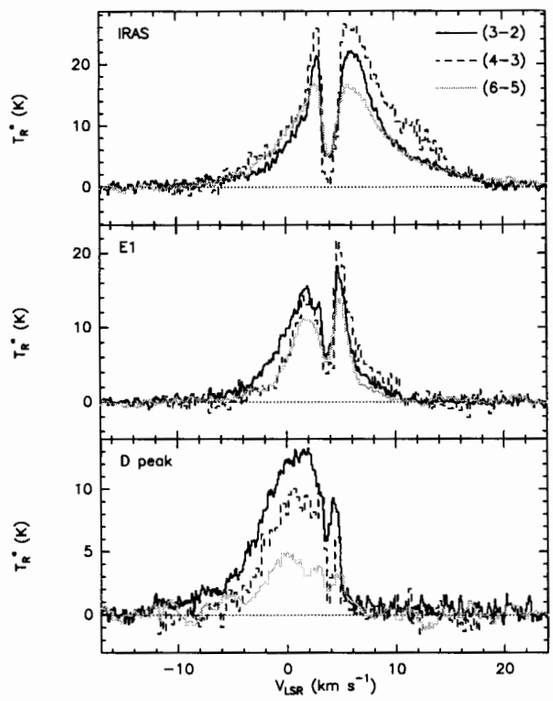

FIG. 2.—Spectra of the CO (3–2), (4–3), and (6–5) emission toward the *IRAS* source, the SiO peak E1, and the deuterium peak (*top to bottom*, respectively). The intensities have been corrected by the corresponding beam efficiencies (65%, 60%, and 60%, respectively). The (3–2) and (4–3) lines have been observed with the 50 MHz spectrometer, while the 500 MHz spectrometer has been used for the (6–5) line.

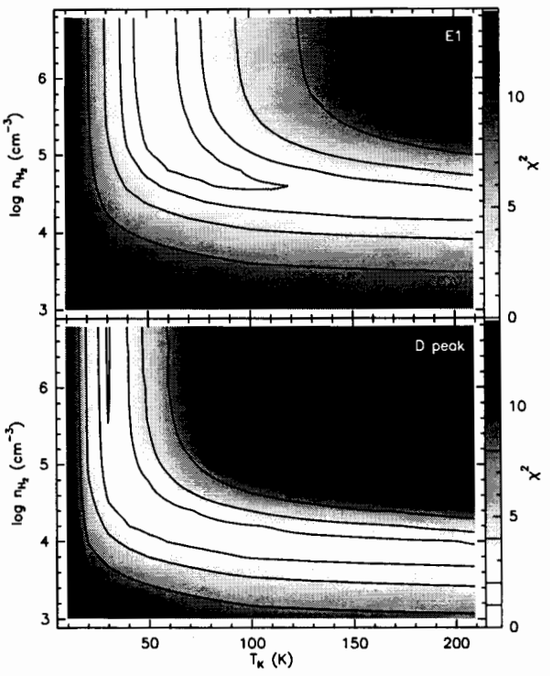

FIG. 3.—Plot of χ^2 corresponding to the observed CO (6–5)/(4–3) and (4–3)/(3–2) line ratios at the E1 and deuterium peak positions as a function of kinetic temperature and H_2 density. Contour levels are 1, 2, 4, and 8. The LVG models were calculated using a CO column density of 1×10^{16} cm^{-2} km^{-1} s. The allowed range of densities and temperatures consistent with the data is not sensitive to the exact value of the column density as the CO emission is optically thin ($\tau < 1$) in this region of the parameter space.

shows the results for $n_H^o = 1 \times 10^4$ cm^{-3}, a preshock density applicable to L1689N [e.g., Menten et al. 1987 derive a density of (2–3) $\times$ 10^4 cm^{-3} in the parent cloud based on their ammonia observations]. The integrated line intensities at the deuterium peak position (Table 1) correspond to 3.9×10^{-6}, 6.7×10^{-6}, and 1.2×10^{-5} ergs cm^{-2} s^{-1} sr^{-1} for the CO (3–2), (4–3), and (6–5) transitions, respectively. These give a good match to the curves corresponding to $v_s \simeq 8$–10 km s^{-1} for a shock propagating along the line of sight (see Fig. 6 of Draine & Roberge 1984). The corresponding line intensities for the E1 position are 4.5×10^{-6}, 1.0×10^{-5}, and 2.5×10^{-5} ergs cm^{-2} s^{-1} sr^{-1}, respectively, indicating a higher shock velocity, $v_s \simeq 15$–25 km s^{-1}.

Schilke et al. (1997) studied the SiO production in the gas phase in C-type shocks with different shock speeds. They conclude that a significant SiO emission is expected for shock velocities greater than ~20 km s^{-1} (see their Fig. 7, top left panel for a preshock gas density of 1×10^4 cm^{-3}). The shock velocities derived above from the intensity of high-J CO lines are thus entirely consistent with the presence of SiO emission at the E1 position and not at the deuterium peak (Hirano et al. 2001).

3.2. *Morphology and Kinematics of Nondeuterated High-Density Tracers*

Figure 4 shows an overlay of HCO^+ (3–2) integrated line intensity (*gray-scale image*), $H^{13}CO^+$ (3–2) integrated inten-

TABLE 1

CO INTENSITIES AND LINE RATIOS

Position	I(3–2)	I(4–3)	I(6–5)	R[(4–3)/(3–2)]	R[(6–5)/(4–3)]	T_k^{min}	$n_{H_2}^{min}$
IRAS.....	189	216	172	1.27 ± 0.23	0.80 ± 0.23	55	2×10^4
E1	108	100	74.2	0.85 ± 0.36	0.80 ± 0.18	35	1×10^4
D peak	91.5	67.6	35.0	0.78 ± 0.06	0.55 ± 0.18	25	5×10^3

NOTE.—Entries in the table are position (see Fig. 1); integrated line intensities of the CO (3–2), (4–3), and (6–5) lines corrected for the corresponding beam efficiencies (K km s^{-1}); the average (4–3)/(3–2) and (6–5)/(4–3) intensity ratios in a 1 km s^{-1} channel (averaged over channels with a signal-to-noise ratio greater than 5 for all three lines) with the corresponding 1 σ uncertainties; and the lower limits for the kinetic temperature (K) and gas density (cm^{-3}) in the outflowing gas. Offsets, with respect to the nominal position, for the three positions observed are (−90″, 20″), (−25″, 25″), and (0, 0), respectively.

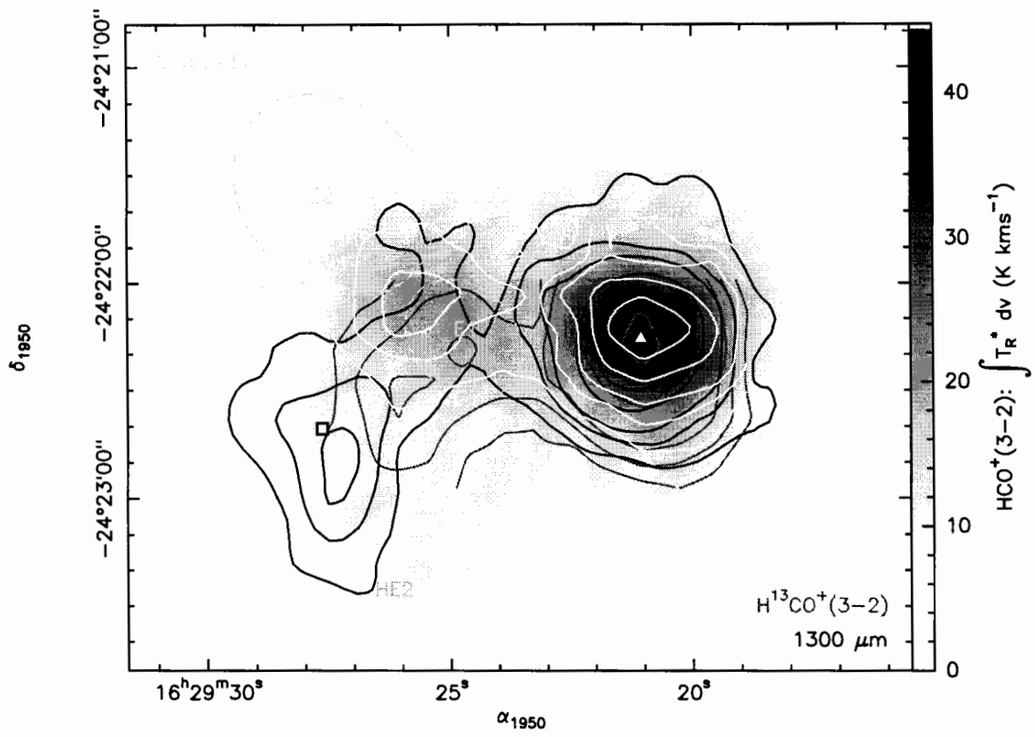

FIG. 4.—Distribution of dense molecular gas in the core of L1689N, as traced by HCO^+ (3–2) emission (*gray-scale image*), 1.3 mm dust continuum emission (*black contours*), $H^{13}CO^+$ (3–2) emission (*gray contours*), and HCN (3–2) emission (*white contours*). Contour levels for the dust continuum are 4%, 6%, 8%, 15%, 30%, 60%, and 90% of the peak (6.7 Jy in a 15″ beam). For $H^{13}CO^+$ (3–2), contour levels are 18%, 26%, 34%, 60%, and 90% of the peak (5.9 K km s^{-1}), and for HCN (3–2), contour levels are 20%, 30%, 40%, 60%, and 80% of the peak (17.5 K km s^{-1}). Light gray dashed ellipses mark the location of SiO (2–1) emission peaks E1 and E2 (Hirano et al. 2001). Symbols mark the location of the *IRAS* source (*triangle*) and the DCO^+ (3–2) peak (*square*; see Fig. 5). The location of the formaldehyde peak HE2 (Castets et al. 2001) is also marked. [*See the electronic edition of the Journal for a color version of this figure.*]

sity (*gray contours*), 1.3 mm dust continuum emission (*black contours*; from F. Motte & P. André 2002, in preparation), and HCN (3–2) integrated intensity (*white contours*). All the tracers peak at the location of the *IRAS* source (*triangle*), with secondary peaks, at 10%–40% level, present to the east/southeast of the main peak. The secondary HCO^+ and HCN emission peaks are associated with the E1 shocked region, and a weak 1.3 mm continuum local maximum is also found at this location. The HCO^+ (3–2) emission peaks near the location of the SiO peak, but it extends farther upstream in the direction of the molecular outflow, in between the E1 and E2 peaks (*light gray dashed ellipses*). The observed displacement between the two tracers can be explained by the nonequilibrium chemistry driven by UV and X-ray photons, which results in greatly enhanced HCO^+ abundances ahead of the shock front (Wolfire & Königl 1993). The less optically thick $H^{13}CO^+$ (3–2) emission (*gray contours*) shows a local maximum near the E1 source, and a second peak ~20″ southeast, at a location where no strong HCO^+, HCN, or SiO emission has been detected. The $H^{13}CO^+$ (1–0) line observed by Hirano et al. (2001) peaks at the southern tip of the $H^{13}CO^+$ (3–2) ridge, indicating the presence of a gradient in the excitation conditions away from the E1 source.

The HCN (3–2) emission peaks farther upstream, along the outflow, in between the SiO peaks E1 and E2. In a recent study of the L1157 molecular outflow, Bachiller et al. (2001) found a prominent chemical segregation between different molecular species, which they attribute to the strong time dependence of the shock chemistry. The E1 region in the L1689N outflow is also a chemically active region characterized by strong formaldehyde and methanol emission, similar to the southern lobe of the L1157 outflow.

The molecular emission in optically thick tracers in the vicinity of the E1 region is generally redshifted by ~1 km s^{-1} with respect to the systemic velocity of the cloud (3.8 km s^{-1}; Fig. 5, *left and right panels* for HCO^+ and HCN emission, respectively). A similar velocity shift was previously seen by Hirano et al. (2001) in the SiO (2–1) emission and was interpreted as evidence of an interaction between the northeastern red lobe of the outflow and the ambient cloud. However, the optically thin $H^{13}CO^+$ (3–2) line peaks near the systemic velocity (3.8–4.1 km s^{-1}; Fig. 6, *left panels*). Some low-level extended molecular emission is seen toward the deuterium peak (*square*), but no localized source can be found at this position in any of the tracers discussed here.

3.3. *Morphology and Kinematics of Deuterated Species*

Figure 6 (*right panels*) shows velocity channel maps of the DCO^+ (3–2) emission. A comparison with the distribution of $H^{13}CO^+$ emission (Fig. 6, *left panels*) is warranted since,

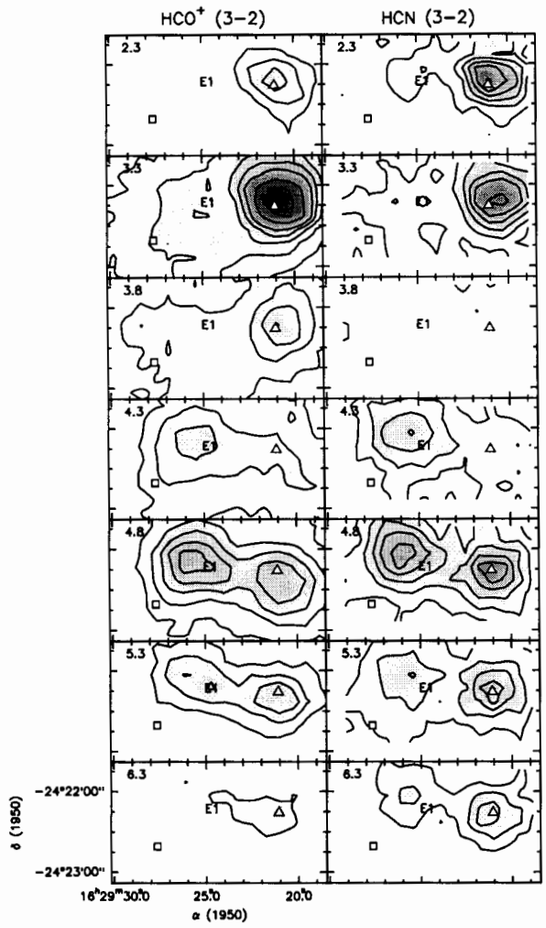

FIG. 5.—Channel maps of the HCO^+ (3–2) and HCN (3–2) emission (*left and right panels*, respectively). Contour levels for HCO^+ are 2, 4, 6, 8, 10, 14, and 18 K km s^{-1}. For HCN, contour levels are 0.5, 1.0, 1.5, 2.0, 2.5, 3.5, and 4.5 K km s^{-1}. Velocities are given in the upper left corner of each panel. Symbols mark the location of the *IRAS* source (*triangle*) and the deuterium peak (*square*).

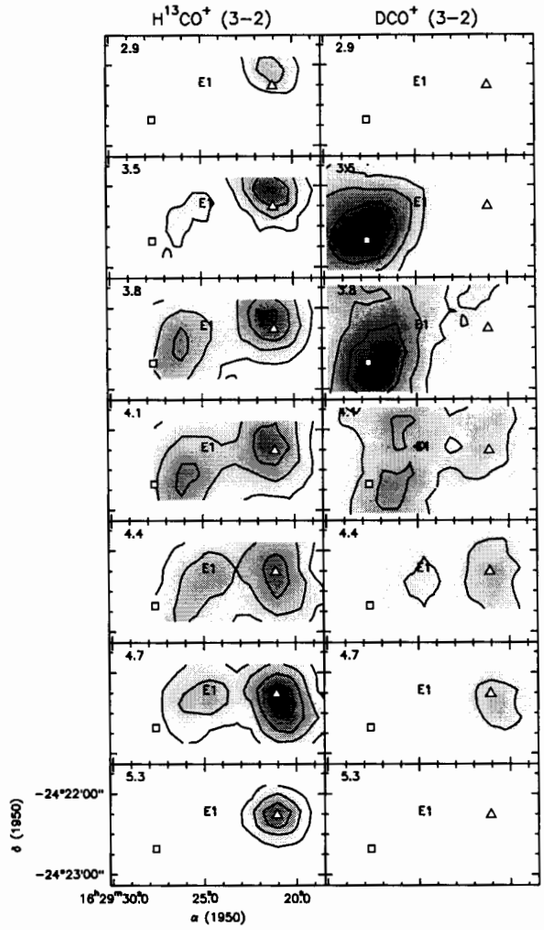

FIG. 6.—Channel maps of the $H^{13}CO^+$ (3–2) and DCO^+ (3–2) emission (*left and right panels*, respectively). Contour levels for $H^{13}CO^+$ are 0.5, 1.0, 1.5, 2.0, 3.5, and 4.5 K km s^{-1}. For DCO^+, contour levels are 1.5–4.5 K km s^{-1} with an interval of 1 K km s^{-1}.

contrary to HCO^+ and HCN, both these lines have at most moderate opacity and should be tracing the same gas. The DCO^+ line is narrower than the $H^{13}CO^+$ line at all positions. However, strong DCO^+ emission is seen in the 3.5 km s^{-1} panel, ~90″ east/southeast of the *IRAS* source, in a region where $H^{13}CO^+$ is relatively weak (*square*). We refer to this position as the deuterium peak. The peculiar kinematics of the deuterated gas is also apparent in the velocity-position cut at a constant right ascension (Fig. 7), which shows a 0.3 km s^{-1} shift between velocities of the DCO^+ and $H^{13}CO^+$ lines, with the DCO^+ emission being blue-shifted with respect to the systemic velocity of the cloud. This effect is not specific to DCO^+, as the same velocity field is seen in DCN (3–2) emission, as well as the limited set of N_2D^+ (3–2) and (4–3) spectra that we have obtained. The observed velocity shift is consistent with the explanation that abundances of deuterated species are strongly enhanced in the molecular gas that is impinged upon and compressed by the eastern blue lobe of the outflow emanating from the *IRAS* source. The gas kinematics is thus analogous to that in the E1 source where the ambient gas is compressed by the northeastern red lobe of the second outflow and redshifted with respect to the systemic velocity of the cloud. The factor of ~3 larger velocity shift observed at the E1 position compared to the deuterium peak is consistent with the faster shock velocity derived from the intensities of high-J CO lines (see § 3.1). A picture thus emerges in which the deuterium peak is a part of the ambient cloud that is pushed and compressed by the outflow. The resulting shock velocity is not sufficient to destroy the grains and release large quantities of silicon into the gas phase. The shock-compressed, dense gas then cools efficiently to low temperatures, and the gas-phase chemistry quickly drives up the abundances of deuterated molecular species. Levels of deuterium fractionation for HCO^+, HCN, and ammonia similar to those observed in L1689N have been found in

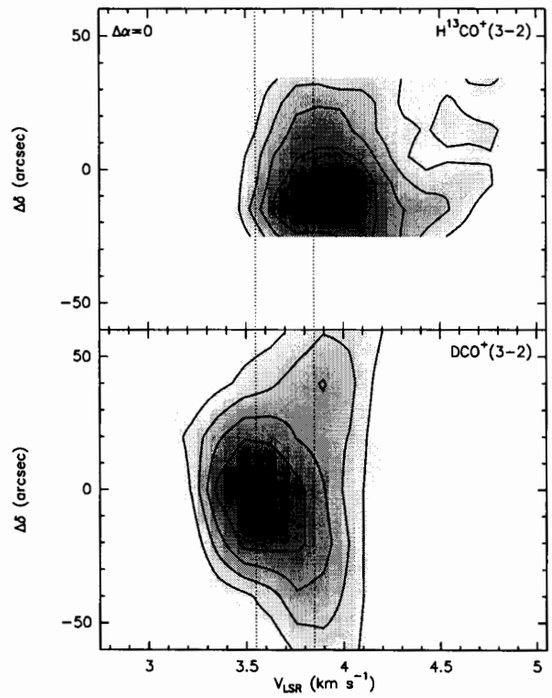

FIG. 7.—Position-velocity cut at $\Delta\alpha = 0$ for the $H^{13}CO^+$ (3–2) and DCO^+ (3–2) emission (*top and bottom panels*, respectively). Contour levels are 30%–90% of the peak with an interval of 15%.

cold dense cores (e.g., Caselli et al. 1998; Tiné et al. 2000; Shah & Wootten 2001). The fractionation reactions responsible for the degree of deuterium enhancement are most efficient at low temperatures. However, chemical models have shown that to reach deuterium abundance levels of ~10%, it is necessary to introduce depletions, i.e., to take into account the freezing of the most abundant gas-phase species onto dust grains (Tiné et al. 2000; Roberts & Millar 2000a, 2000b). Freezing occurs fast in collapsing cores (Aikawa et al. 2001) and results in very high levels of fractionation on a short timescale. L1689N shows similar properties to the dense protostellar core L1544 (Caselli et al. 2002 and references therein) and could be another example of a dense prestellar core on the verge of forming stars.

A relatively strong 1.3 mm continuum peak (~0.6 Jy in a 15″ beam) is located ~90″ east/southeast from the *IRAS* source in the general vicinity of the deuterium peak (Fig. 4). Castets et al. (2002) and Loinard et al. (2001) suggested that this source is a class 0 protostar driving a molecular outflow independent of the two outflows emanating from the *IRAS* source. We find no evidence in our data to support this conclusion. The continuum source is spatially resolved at 1.3 mm (~25″ × 50″ FWHM) and is not coincident with any near- or far-infrared source. Based on their 2.7 mm continuum interferometric observations, A. Wootten et al. (2002, in preparation) conclude that any compact dust source embedded in the molecular core contains less than a few percent of the total molecular mass. VLA observations of Wootten (1989) have not revealed the presence of a radio continuum source associated with the 1.3 mm continuum peak at 1 σ flux levels of ~25 and 50 μJy at 6 and 2 cm, respectively (A. Wootten 2001, private communication). However, we note that the class 0 protostar IRAM 04191+1522 (André, Motte, & Bacmann 1999) would not have been detected at these flux levels. More sensitive radio continuum observations are required to determine the exact evolutionary state of the continuum source near the deuterium peak in L1689N. However, the existing data are consistent with the idea that this source is a prestellar dense core. Similar conclusions have been reached by R. Stark et al. (2002, in preparation), who imaged the region at shorter submillimeter wavelengths with SCUBA. They conclude that the secondary dust source is a pre-protostellar core with a dust temperature of 12 K and a mean density of 1.8×10^6 cm^{-3}, which may hide what they refer to as a "class −I protostar, deeply embedded in a still unaffected cold core (see Boss & Yorke 1995)."

Given the fact that the secondary continuum source in L1689N is not coincident with the emission peak of the deuterated molecules (~10″ offset; see Fig. 4; note that the DCO^+ peak is located in between the two NH_3 peaks detected by Wootten & Loren 1987) and is not seen at all in other high-density molecular tracers, it is unclear whether there is any direct physical association between the dust continuum source and the deuterium peak. In particular, it is not clear whether the high volume density derived by R. Stark et al. (2002, in preparation) from their submillimeter continuum observations, a factor of 3–4 higher than the

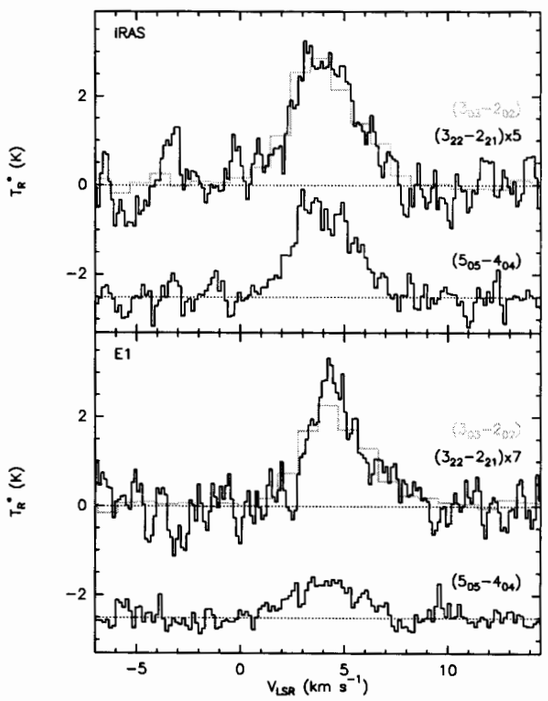

FIG. 8.—Spectra of the H_2CO (3_{03}–2_{02}) (*gray line*), (3_{22}–2_{21}) (*upper black line*), and (5_{05}–4_{04}) emission (*lower black line*, shifted down by 2.5 K) at the *IRAS* and E1 positions (*top and bottom panels*, respectively). The (3_{22}–2_{21}) spectra have been multiplied by a factor of 5 and 7 at the *IRAS* and E1 positions, respectively.

TABLE 2

FORMALDEHYDE INTENSITIES AND LINE RATIOS

Position	$I(3_{03}-2_{02})$	$I(3_{22}-2_{21})$	$I(5_{05}-4_{04})$	$R(3_{03}/3_{32})$	$R(5_{05}/3_{03})$	T_k	n_{H_2}
IRAS.....	11.2	2.2	7.3	5.1	0.65	65	2.5×10^6
E1	8.3	1.2	2.9	7.0	0.35	45	1.8×10^6
D peak	2.2	<0.15	<0.9	> 14	<0.42	$\lesssim 27$	...
HE2	5.7	0.72	...	7.9	...	~ 37	...

NOTE.—Entries in the table are position (see Fig. 1); integrated line intensities of the $(3_{03}-2_{02})$, $(3_{22}-2_{21})$, and $(5_{05}-4_{04})$ lines ($\int T_R^* dv$, K km s^{-1}); the $(3_{03}-2_{02})/(3_{22}-2_{21})$ and $(5_{05}-4_{04})/(3_{03}-2_{02})$ intensity ratios; and the gas kinetic temperature (K) and density (cm^{-3}) derived from LVG models. A five-point cross scan with a 15″ spacing was observed at each position in the $(5_{05}-4_{04})$ line, and the resulting spectra were convolved to the 35″ beam size of the $(3_{03}-2_{02})$ line. The opacity of the formaldehyde lines has not been measured directly, but the observed intensity of the $(3_{03}-2_{02})$ line indicates optical depths $\lesssim 0.5$ at all positions. The $(3_{22}-2_{21})$ and $(5_{05}-4_{04})$ lines are not detected at the deuterium peak position. The values given in the table are 3 σ upper limits for the integrated line intensity. The HE2 position corresponds to a secondary H_2CO peak (Castets et al. 2001). Offsets, with respect to the nominal position, for the four positions observed are (−90″, 20″), (−40″, 20″), (0, −8″), and (−20″, −53″), respectively.

TABLE 3

HCO$^+$ ISOTOPOMERIC RATIOS

Position	$I(HCO^+)$	$I(H^{13}CO^+)$	$I(DCO^+)$	$R(DCO^+/H^{13}CO^+)$	$R(DCO^+/HCO^+)$
IRAS.....	39.8	5.81	3.40	0.45	0.7×10^{-2}
E1	21.8	2.06	2.55	1.1	1.8×10^{-2}
D peak	5.72	1.25	3.29	5.0	8.1×10^{-2}

NOTE.—Entries in the table are position (see Fig. 1); integrated line intensities of the HCO$^+$ (3–2), H^{13}CO$^+$ (3–2), and DCO$^+$ (3–2) lines ($\int T_R^* dv$, K km s^{-1}); and the DCO$^+$/H^{13}CO$^+$ and DCO$^+$/HCO$^+$ abundance ratios. The observed HCO$^+$/H^{13}CO$^+$ intensity ratios of 5–7 imply H^{13}CO$^+$ optical depths averaged across the line of ~0.1–0.24 assuming a $^{12}C/^{13}C$ isotopic ratio of 62 (Langer & Penzias 1993). The DCO$^+$/HCO$^+$ column density ratio is based on LVG models with the kinetic temperatures and gas densities derived from the formaldehyde data (§ 3.4). The high DCO$^+$ brightness temperature observed at the deuterium peak position (~4.2 K; see Fig. 10) indicates that the emission is moderately optically thick ($\tau \sim 2$ for $T_k = 12$ K; the corresponding optical depth of H^{13}CO$^+$ is ~0.4; this optical depth difference between the two species results in an ~50% correction to the observed intensity ratio and has been included in the table). Typical modeling uncertainties are ~20%. Adding in quadrature 25% calibration uncertainties for each line leads to a combined uncertainty of ~40% for the derived D/H ratio at the *IRAS* and E1 positions. At the deuterium peak position an additional ~30% uncertainty owing to the DCO$^+$ optical depth has to be included, leading to a combined uncertainty of ~50%. The DCO$^+$/HCO$^+$ abundance ratio assumes an HCO$^+$/H^{13}CO$^+$ ratio of 62.

TABLE 4

HCN ISOTOPOMERIC RATIOS

Position	I(HCN)	$I(H^{13}CN)$	I(DCN)	R(DCN/H^{13}CN)	R(DCN/HCN)
IRAS.....	19.6	2.25	1.88	0.72	1.2×10^{-2}
E1	5.46	0.57	0.54	1.0	1.6×10^{-2}
D peak	2.35	0.10	0.49	7.0	1.1×10^{-1}

NOTE.—Entries in the table are position (see Fig. 1); integrated line intensities of the HCN (3–2), H^{13}CN (3–2), and DCN (3–2) lines ($\int T_R^* dv$, K km s^{-1}); and the DCN/H^{13}CN and DCN/HCN abundance ratios. The observed HCN/H^{13}CN intensity ratio of ~9 implies an HCN optical depth averaged across the line of ~7.7 toward the *IRAS* and E1 positions, assuming a $^{12}C/^{13}C$ isotopic ratio of 62 (Langer & Penzias 1993). The HCN optical depth toward the deuterium peak is ~2.6. The H^{13}CN emission is thus optically thin at all positions. The red shoulder in the DCN (3–2) spectrum at the deuterium peak position (Fig. 10, *bottom panel*) is owing to the hyperfine splitting. The observed hyperfine ratio of 0.32 ± 0.05 (1 σ uncertainty) is statistically consistent with the optically thin ratio of 0.25. The DCN/H^{13}CN column density ratio is based on LVG models with the kinetic temperatures and gas densities derived from the formaldehyde data (§ 3.4). Typical modeling uncertainties are ~20%. Adding in quadrature 25% calibration uncertainties for each line leads to a combined uncertainty of ~40% for the derived D/H ratio at all positions. The DCN/HCN abundance ratio assumes an HCN/H^{13}CN ratio of 62.

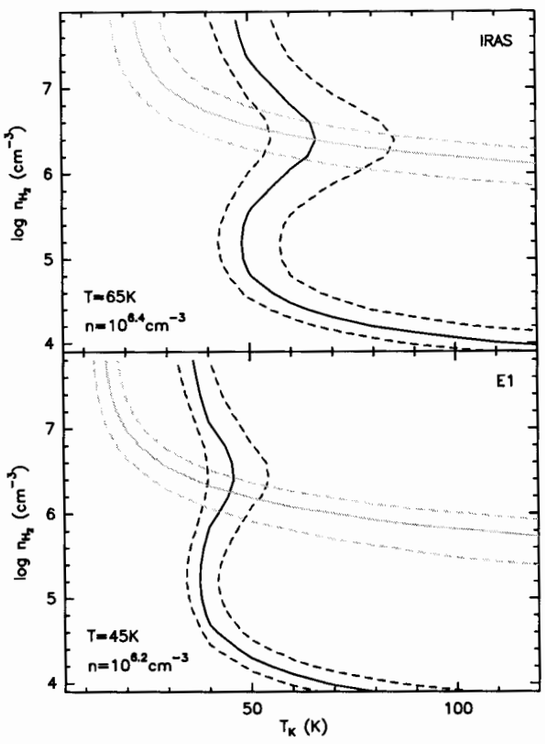

FIG. 9.—LVG model computations of the $(3_{03}–2_{02})/(3_{23}–2_{21})$ and $(5_{05}–4_{04})/(3_{03}–2_{02})$ intensity ratios of paraformaldehyde (*black and gray lines*, respectively). The H_2CO column density is 1×10^{13} cm^{-3}. The solid lines correspond to the observed ratios at the *IRAS* and E1 positions (*top and bottom panels*, respectively). The dashed lines outline the allowed range of temperatures and densities given the observational uncertainties of 15% and 35% for the $(3_{03}–2_{02})/(3_{23}–2_{21})$ and $(5_{05}–4_{04})/(3_{03}–2_{02})$ line ratios, respectively.

value used in our LVG computations (see § 3.4), is also applicable to the deuterium source.

3.4. *Excitation Conditions in Dense Molecular Gas*

The excitation conditions derived from observations of high-J CO lines (§ 3.1) apply to the high-velocity gas in the molecular outflow and may not be representative for the dense gas traced by the HCO^+ and HCN emission (§ 3.2). To independently estimate the kinetic temperature and density in these regions, we have observed at selected positions the $(3_{03}–2_{02})$, $(3_{23}–2_{21})$, and $(5_{05}–4_{04})$ lines of paraformaldehyde. As discussed by Mangum, Wootten, & Plambeck (1993), this combination of lines provides a good measure of the excitation conditions for H_2 densities $\gtrsim 10^5$ cm^{-3} and kinetic temperatures $\lesssim 50$ K. Table 2 gives observed integrated line intensities corrected for the corresponding beam efficiencies together with the intensity ratios, and the observed spectra at the *IRAS* and E1 positions are shown in Figure 8. We have computed a grid of LVG models for a range of gas densities and kinetic temperatures and show in Figure 9 contours corresponding to the observed line ratios on the T_k-n_{H_2} plane (*solid lines*). The $(3_{03}–2_{02})$ and $(3_{23}–2_{21})$ lines are observed together in a single spectrum, and the uncertainty of the observed line ratio that measures the gas kinetic temperature is ~15%, while the uncertainty of the $(5_{05}–4_{04})/(3_{03}–2_{02})$ ratio that provides a measure of the gas density is ~35%. Dotted lines in Figure 9 outline the range of temperatures and densities consistent with the data, given these uncertainties. We derive a kinetic temperature of 45 K and a density of $\sim 1.8 \times 10^6$ cm^{-3} at the E1 position with uncertainties of ~(−7, 10) K for T_k and ~0.25 for $\log n_{H_2}$. The excitation conditions are not as well constrained by the data at the *IRAS* position, where we derive a kinetic temperature of 65 (−10, 20) K and a density of $\sim 2.5 \times 10^6$ cm^{-3} with an uncertainty of ~0.25 on the log scale. The kinetic temperatures derived here are typically ~10 K lower than those in the outflowing gas based on the CO data (§ 3.1).

The $(5_{05}–4_{04})$ line is not detected at the deuterium peak position, and no meaningful density estimate can be derived there. The upper limit of 14 for the $(3_{03}–2_{02})/(3_{23}–2_{21})$ line ratio implies a kinetic temperature of $\lesssim 27$ K there. In the subsequent analysis we use a kinetic temperature of 12 K at the deuterium peak position (based on NH_3 observations of Menten et al. 1987) and a density of 5×10^5 cm^{-3}, consistent with the observed DCO^+ (5–4)/(3–2) and N_2D^+ (4–3)/(3–2) line intensity ratios, as well as the observed velocity broadening of the DCO^+ (3–2) line compared to the optically thin (5–4) line. This density corresponds to a factor of ~20 enhancement compared to the density in the parent molecular cloud based on NH_3 observations.

3.5. *Molecular Abundances of Deuterated Species*

High-resolution spectra of HCO^+ and HCN isotopomers at the *IRAS*, E1, and deuterium peak positions are shown in Figures 10 and 11, respectively, and Tables 3 and 4 give the observed line intensities. The data have been analyzed in the framework of LVG models using the excitation conditions determined in § 3.4, to derive the DCO^+/HCO^+ and DCN/HCN column density ratios at the three positions. The D/H ratios derived from the $H^{13}CO^+$ and $H^{13}CN$ data agree to within a factor of $\lesssim 1.6$ at any given position. The D/H ratio at the E1 position is a factor of ~1.8 higher than that at the *IRAS* position, while a factor of ~10 deuterium enhancement compared to the *IRAS* position is found at the deuterium peak. The D/H ratios in HCO^+ and HCN of ~1%–11% derived here are in the same range as the values compiled by Loinard et al. (2001) based on formaldehyde, ammonia, and HCO^+ observations (0.3%–18%), as well as those derived by Hirota et al. (2001) based on HNC and HCO^+ observations and Turner (2001) (~1%–14%). These values fall within the range of predictions of gas-phase chemical models for dense and cold gas, provided that significant accretion of CO and other chemically important species has occurred onto the dust grains (Roberts & Millar 2000a, 2000b). Loinard et al. (2001) argue for little or no CO depletion in L1689N. However, the limited $C^{18}O$ (2–1) mapping we have carried out shows a rather striking anticorrelation between the distributions of the DCO^+ (3–2) and $C^{18}O$ (2–1) emission at velocities of 3.5–3.8 km s^{-1} in the vicinity of the deuterium peak. The observed intensity of the $C^{18}O$ (2–1) emission toward the deuterium peak (6.6 K km s^{-1} integrated line intensity, 5.7 K brightness temperature) implies a $C^{18}O$ column density of 7×10^{15} cm^{-2}, assuming a kinetic temperature of 12 K and a gas density of

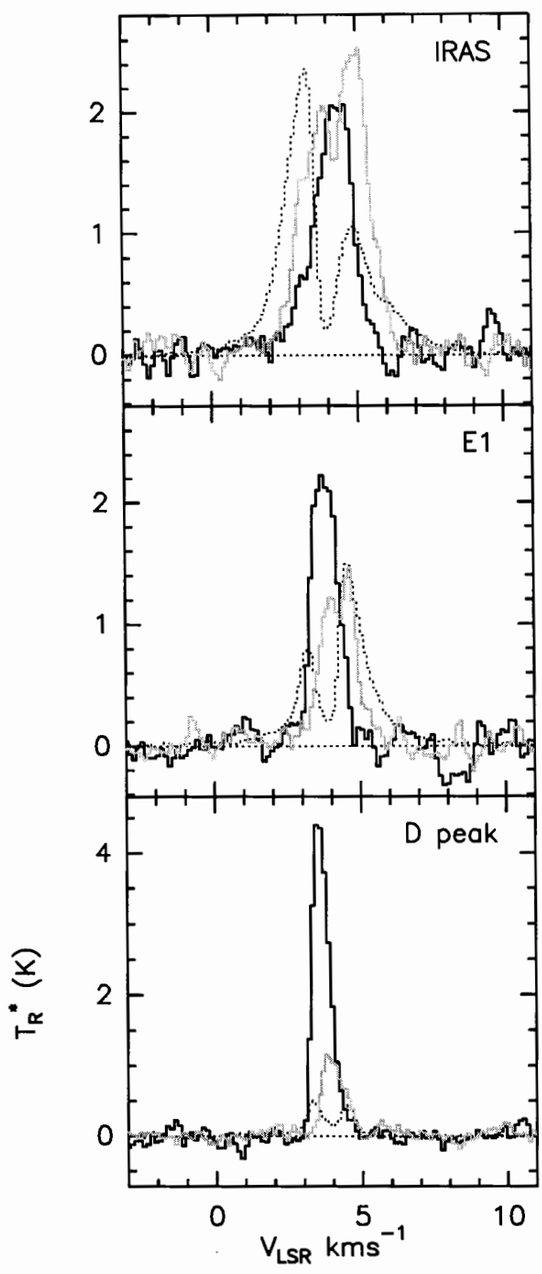

FIG. 10.—Spectra of DCO^+ (3–2) (*solid black lines*), HCO^+ (3–2) (divided by 8; *dotted lines*), and $H^{13}CO^+$ (3–2) (*solid gray lines*) at the *IRAS*, E1, and deuterium peak position (*top to bottom*, respectively).

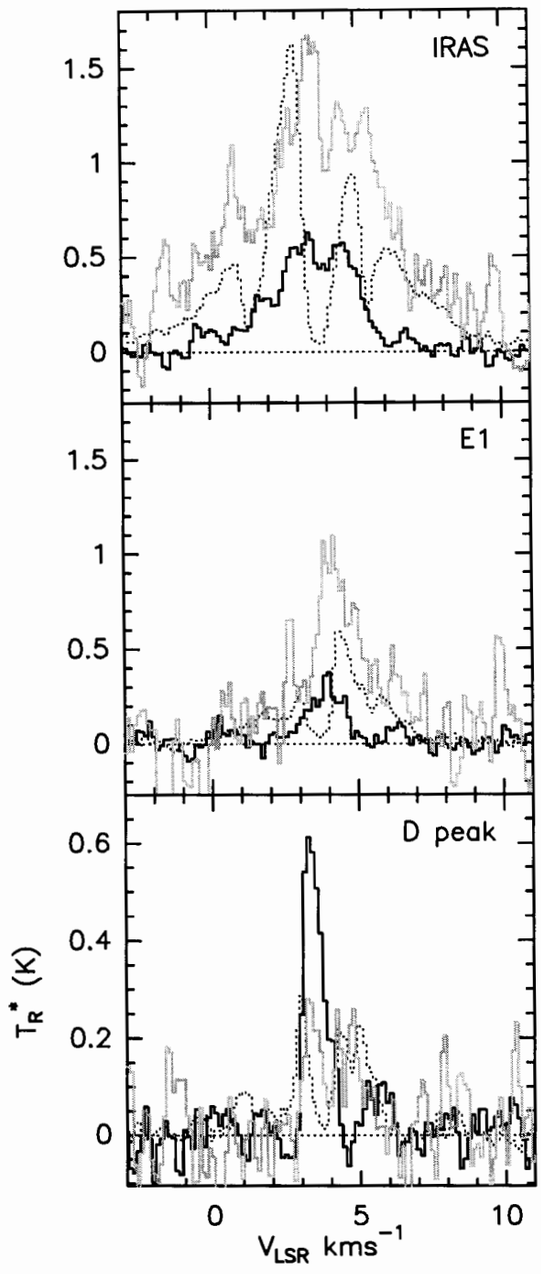

FIG. 11.—Spectra of DCN (3–2) (*solid black lines*), HCN (3–2) (divided by 4; *dotted lines*), and $H^{13}CN$ (3–2) (multiplied by 4; *solid gray lines*) at the *IRAS*, E1, and deuterium peak position (*top to bottom*, respectively).

5×10^5 cm^{-3}. $C^{18}O$ emission is moderately optically thick with the line center optical depth of ~1.55, based on LVG models. The 1.3 mm dust continuum flux at the same location is ~0.5 Jy in a 15″ beam and ~1.8 Jy in a 31″ beam corresponding to the angular resolution of the $C^{18}O$ (2–1) data. Assuming a temperature of 12 K (R. Stark et al. 2002, in preparation) and a mass opacity coefficient of 0.005 cm^2 g^{-1} (appropriate for prestellar dense clumps and cores; see Motte, André, & Neri 1998 and references therein), we derive an H_2 column density of 2.8×10^{23} cm^{-2} in a 31″ beam. This leads to a $C^{18}O$ fractional abundance of 2.5×10^{-8} at the deuterium peak, a factor of ~7 lower than

the canonical value of 1.7×10^{-7} (Frerking, Langer, & Wilson 1982). Such a depletion level is sufficient to produce the observed deuterium fractionation of HCN and HCO^+ in the framework of gas-phase chemical models.

While the deuterium fractionation levels we derive here for HCN and HCO^+ are within the range of gas-phase model predictions, some quantitative discrepancies between the observations and model predictions remain. For example, we derive a higher deuterium fractionation in HCN compared to HCO^+, by about 35% at the deuterium peak, while the gas-phase chemical models predict the fractionation to be higher in HCO^+, typically by a factor of $\sim$2 (e.g., Roberts & Millar 2000a). While such discrepancies may be at least partially attributed to the observational and modeling uncertainties, it is worth pointing out that Turner (2001) also derives a higher deuterium fractionation in HCN compared to HCO^+ in L183, where deuterium fractionation levels comparable to those in L1689N are observed.

The very high D/H ratio in doubly deuterated formaldehyde at the L1689N deuterium peak position (40% $\pm$ 20%; Loinard et al. 2001) is outside of the gas-phase model predictions. However, as discussed by Loinard et al. (2001), the current grain surface chemistry models also find it difficult to explain the observed fractionation levels in doubly deuterated formaldehyde in this source.

4. SUMMARY

We have studied the morphology, kinematics, and excitation conditions of the dense molecular gas in the core of L1689N. We find the E1 shocked region in the northeastern red lobe of the L1689N outflow to be a chemically active region, characterized by strong formaldehyde emission, with a spatial stratification similar to that found in the southern lobe of the L1157 outflow. Using LVG models, we derive D/H ratios in HCO^+ and HCN at the positions of IRAS 16293–2422, the E1 shock, and the deuterium peak. The two ratios agree to within a factor of $\lesssim$1.6 at any given position. They are typically $\sim$1% at the *IRAS* source and E1 positions, with an order of magnitude higher ratios of 8%–11% derived at the deuterium peak. The high deuterium fractionation at this position agrees with the values previously measured in DNC and ammonia ($[DNC]/[HNC] \simeq [NH_2D]/[NH_3] \simeq 9\%$). These values fall within the range of predictions of gas-phase chemical models for dense and cold gas, provided that significant accretion of CO and other chemically important species has occurred onto the dust grains (Roberts & Millar 2000a, 2000b). However, some quantitative discrepancies between the observations and model predictions remain. For example, contrary to gas-phase model predictions, we derive a

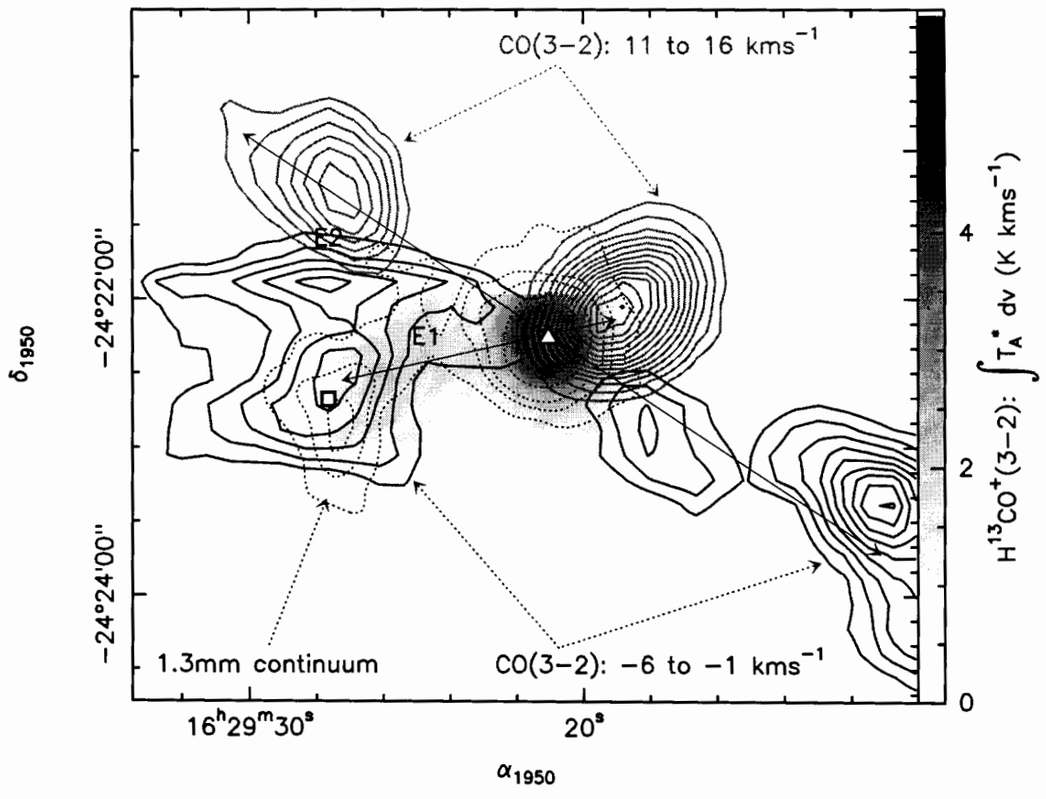

FIG. 12.—Overall morphology of the L1689N core: $H^{13}CO^+$ (3–2) integrated line intensity (*gray-scale image*), 1.3 mm dust continuum emission (*black dotted contours*), and high-velocity CO (3–2) emission (−6 to −1 km s^{-1} and 11–16 km s^{-1}; *black and gray contours*, respectively). Symbols mark the location of the *IRAS* source (*triangle*) and the deuterium peak (*square*). Arrows show the direction of the two outflows emanating from the *IRAS* source. The deuterium peak is associated with the eastern blue outflow lobe. [*See the electronic edition of the Journal for a color version of this figure.*]

higher deuterium fractionation in HCN compared to HCO^+. Better constraints on the kinetic temperature in this region are needed to improve the comparison with models, since the fractionation is extremely sensitive to the kinetic temperature. The lower D/H values observed toward the E1 and *IRAS* positions are consistent with the higher kinetic temperature and gas density in these active regions compared to the more quiescent deuterium peak in L1689N.

The location of the deuterium peak within the eastern blue lobe of the molecular outflow emanating from IRAS 16293−2422 and the observed velocity shift of deuterated species at this location with respect to the systemic velocity of the cloud suggest that the deuterium peak is an interaction region between the outflow and the ambient cloud (Fig. 12), similar to that at the E1 position. The relatively low shock velocity of 8–10 km s^{-1} derived at this location from the observed intensities of high-J CO lines explains why no SiO emission has been detected there. A minimum shock velocity of $\sim$20 km s^{-1}, similar to that derived at the E1 position, is required to release significant quantities of silicon into the gas phase.

This research has been supported by NSF grant AST-9980846 to the Caltech Submillimeter Observatory. We thank J. Cernicharo for providing us with an LVG code for the molecules studied here, R. Peng for taking the CO (3–2) data, and A. Wootten and G. Sandell for sending us manuscripts prior to publication.

REFERENCES

Aikawa, Y., Ohashi, N., Imtsuka, S., Herbst, E., & Takakuwa, S. 2001, ApJ, 552, 639
André, P., Motte, F., & Bacmann, A. 1999, ApJ, 513, L57
Bachiller, R., Guiterea, M., Kumar, M. S. N., & Tafalla, M. 2001, A&A, 372, 899
Blake, G. A., van Dishoeck, E. F., Jansen, D. J., Groesbeck, T. D., & Mundy, L. G. 1994, ApJ, 428, 680
Boss, A. P., & Yorke, H. W. 1995, ApJ, 439, L55
Caselli, P., Walmsley, C. M., Terzevia, R., & Herbst, E. 1998, ApJ, 499, 234
Caselli, P., Walmsley, C. M., Zucconi, A., Tafalla, M., Dore, L., & Myers, P. C. 2002, ApJ, 565, 344
Castets, A., Ceccarelli, C., Loinard, L., Caux, E., & Lefloch, B. 2001, A&A, 375, 40
Ceccarelli, C., Castets, A., Caux, E., Hollenbach, D., Loinard, L., Molinari, S., & Tielens, A. G. G. M. 2000a, A&A, 355, 1129
Ceccarelli, C., Loinard, L., Castets, A., Tielens, A. G. G. M., & Caux, E. 2000b, A&A, 357, L9
Ceccarelli, C., Loinard, L., Castets, A., Tielens, A. G. G. M., Caux, E., Lefloch, B., & Vastel, C. 2001, A&A, 372, 998
Draine, B. T., & Roberge, W. G. 1984, ApJ, 282, 491
Frerking, M. A., Langer, W. D., & Wilson, R. W. 1982, ApJ, 262, 590
Gerin, M., Wootten, H. A., Combes, F., Boulanger, F., Peters, W. L., III, Kuiper, T. B. H., Encrenaz, P. J., & Bogey, M. 1987, A&A, 173, L1
Hirano, N., et al. 2001, ApJ, 547, 899
Hirota, T., Ikeda, M., & Yamamoto, S. 2001, ApJ, 547, 814
Langer, W. D., & Penzias, A. A. 1993, ApJ, 408, 539
Loinard, L., Castets, A., Ceccarelli, C., Caux, E., & Tielens, A. G. G. M. 2001, ApJ, 552, L163
Loinard, L., Castets, A., Ceccarelli, C., Tielens, A. G. G. M., Faure, A., Caux, E., & Duvert, G. 2000, A&A, 359, 1169
Loren, R. B., Wootten, A., & Wilking, B. A. 1990, ApJ, 365, 269
Mangum, J. G., Wootten, A., & Plambeck, R. L. 1993, ApJ, 409, 282
Menten, K. M., Serabyn, E., Güsten, R., & Wilson, T. L. 1987, A&A, 177, L57
Mizuno, A., Fukui, Y., Iwata, T., & Nozawa, S. 1990, ApJ, 356, 184
Motte, F., André, P., & Neri, R. 1998, A&A, 336, 150
Mundy, L. G., Wootten, A., Wilking, B. A., Blake, G. A., & Sargent, A. I. 1992, ApJ, 385, 306
Roberts, H., & Millar, T. J. 2000a, A&A, 361, 388
———. 2000b, A&A, 364, 780
Rodgers, S. D., & Charnley, S. B. 2001, ApJ, 553, 613
Saito, S., Ozeki, H., Ohishi, M., & Yamamoto, S. 2000, ApJ, 535, 227
Schilke, P., Walmsley, C. M., Pineau des Forêts, G., & Flower, D. R. 1997, A&A, 321, 293
Shah, R. Y., & Wootten, A. 2001, ApJ, 554, 933
Tiné, S., Roueff, E., Falgarone, E., Gerin, M., & Pineau des Forêts, G. 2000, A&A, 356, 1039
Turner, B. 2001, ApJS, 136, 579
van Dishoeck, E. F., Blake, G. A., Jansen, D. J., & Groesbeck, T. D. 1995, ApJ, 447, 760
Walker, C. K., Lada, C. J., Young, E. T., Maloney, P. R., & Wilking, B. A. 1986, ApJ, 309, L47
Wolfire, M. G., & Königl, A. 1993, ApJ, 415, 204
Wootten, A. 1989, ApJ, 337, 858
Wootten, A., & Loren, R. B. 1987, ApJ, 317, 220